Optics Letters

Visible light OCT improves imaging through a highly scattering retinal pigment epithelial wall

Tingwei Zhang,[1] Aaron M. Kho,[1] Robert J. Zawadzki,[2] Ravi S. Jonnal,[2] Glenn Yiu,[2] and Vivek J. Srinivasan[1,2,*]

[1]Department of Biomedical Engineering, University of California Davis, Davis, California 95616, USA
[2]Department of Ophthalmology and Vision Science, University of California Davis, Davis School of Medicine, Sacramento, California 96817, USA
*Corresponding author: vjsriniv@ucdavis.edu

Received 13 August 2020; revised 9 September 2020; accepted 21 September 2020; posted 22 September 2020 (Doc. ID 405398); published 23 October 2020

Here we provide a counter-example to the conventional wisdom in biomedical optics that longer wavelengths aid deeper imaging in tissue. Specifically, we investigate visible light optical coherence tomography of Bruch's membrane (BM) in the non-pathologic eyes of humans and two mouse strains. Surprisingly, we find that shorter visible wavelengths improve the visualization of BM in pigmented eyes, where it is located behind a highly scattering layer of melanosomes in the retinal pigment epithelium (RPE). Monte Carlo simulations of radiative transport suggest that, while absorption and scattering are higher at shorter wavelengths, detected multiply scattered light from the RPE is preferentially attenuated relative to detected backscattered light from the BM.

https://doi.org/10.1364/OL.405398

Histopathology suggests that early ocular changes in aging and age-related macular degeneration (AMD) occur on the micron scale between the retinal pigment epithelium (RPE) and Bruch's membrane (BM), a multilayered structure that mediates transport between the RPE and choriocapillaris (CC). The early stages of dry AMD are characterized by soft drusen and basal linear deposits between the RPE basement membrane and inner collagenous layer (ICL) of BM [1]. Typically BM is just 2–4 μm thick in adult humans [2], less than 1 μm thick in mice [3], and normally situated directly under the RPE.

In vivo delineation of BM in non-pathologic, pigmented eyes has been challenging for near-infrared (NIR) optical coherence tomography (OCT) systems, which utilize > 700 nm wavelengths, though recent research-grade ultrahigh resolution NIR systems have made some progress [4]. In clinical NIR OCT, hyper-reflective BM and RPE bands are sometimes individually detectable *in vivo*, but only if their close anatomical relationship is perturbed, for instance, by RPE elevation, atrophy, or pigmentation loss. In the absence of such overt pathology, clinical NIR OCT typically detects a single hyper-reflective RPE/BM complex [5]. The difficulty of imaging a BM in pigmented eyes may relate to its anatomical location beneath the RPE, which contains a highly scattering [6] and depolarizing [7] layer of melanosomes, which are melanin-containing organelles. Some absorption and scattering properties of melanosomes may be shared with melanolipofuscin granules, which can outnumber RPE melanosomes in older eyes [8].

Conventional wisdom in biomedical optics states that longer wavelengths image deeper in tissue. This useful rule-of-thumb is founded on the overall decrease in absorption of biological chromophores and tissue scattering with wavelengths [9], particularly from the visible to the infrared. In this Letter, motivated by the theoretical micron-scale axial resolution of visible light OCT [10], now achievable *in vivo* [11,12], we investigate visible light OCT of BM in the eyes of normal, pigmented humans, as well as pigmented and unpigmented mice. We find that visible light OCT consistently depicts well-separated hyper-reflective bands corresponding to the BM and the RPE *in vivo*, as might be expected with high axial resolution. We further find that, contrary to conventional wisdom, shorter visible wavelengths improve the distinction between the BM band and the highly scattering, melanin-rich RPE band, even at the same axial resolution. The latter finding is unexpected as both tissue scattering and absorption of all relevant chromophores increase at shorter visible wavelengths. Based on a simple Monte Carlo simulation, we propose two explanations: (1) absorption of RPE melanin and (2) melanosome scattering anisotropy (g). Both effects preferentially attenuate the haze of multiply scattered RPE light relative to useful backscattered light, which travels to and from BM ballistically or quasi-ballistically, and both effects are expected to increase at shorter wavelengths.

Twenty-nine human subjects (21–57 years old, 13 female) with no history of ocular pathology were imaged on a prototype visible light OCT system developed at UC Davis [12]. Additionally, pigmented (C57BL/6 J) and albino, i.e., melanin-free, (BALB/cJ) mice (The Jackson Laboratory) were imaged by a mouse visible light OCT system [11] to assess the impact of melanin pigment on BM visualization. Procedures were approved by the UC Davis Institutional Review Board and Animal Care and Use Committee, respectively.

Raw OCT interference fringes were resampled to linear wavenumber space, dispersion compensated, spectrally shaped, Fourier transformed, and corrected for motion [11,12]. Images were averaged on an intensity basis prior to display on a square root (amplitude) scale. After Gaussian shaping of the OCT

spectrum, the axial resolution was measured to be 1.0 μm in tissue. To also assess wavelength dependence of OCT image contrast, raw OCT data were also re-processed by digital shaping to achieve spectrally narrower orange and green subbands (Fig. 1B). Each subband color was assigned based on its central wavelength. The axial resolution of the re-processed subband images was 2.0 μm in tissue due to the narrower spectral width of each subband. Cross-sectional images based on the total spectrum and respective subbands were compared qualitatively. Additionally, intensity profiles versus depth were corrected for the noise offset, normalized, averaged, and compared. To assess BM visualization, BM contrast was quantified as the intensity ratio of the BM peak to the basal RPE valley in the fovea and parafovea.

Observations in a 27 year-old Caucasian female subject, with a brown-colored iris (Figs. 1A and 1E), showed a clear separation between the hyper-reflective RPE band and BM. A similar separation was noted in 28 out of the 29 normal human eyes imaged on our prototype visible light OCT system (confirmed by two independent observers). Furthermore, this separation was more prominent for green than for orange light, as shown in both cross-sectional images and normalized intensity profiles (Figs. 1E and 1F). Excluding four subjects with poor subband image quality and seven subjects imaged with an earlier, red-shifted spectrometer alignment, BM subband contrast was quantified in 18 subjects (21–57 years old, 10 female). Every single subject exhibited improved BM contrast in the short wavelength subband (Fig. 1C), which was not explained simply by RPE reflectivity differences (Fig. 1D). We next imaged pigmented and unpigmented mice on a different visible light OCT system [11]. The RPE in the pigmented mouse was hyper-reflective (Fig. 2A), while the RPE in the unpigmented mouse was hypo-reflective (Fig. 2D), suggesting that melanosomes with melanin are the main source of scattering in RPE at these wavelengths, confirming earlier work [7,14]. For green light, the gap between the hyper-reflective, pigmented RPE band (bracket) and the BM band (arrows) was more prominent, and BM contrast was higher than for orange light (Figs. 2B and 2C), suggesting the BM is visualized better with shorter wavelengths. However, in the hypo-reflective, unpigmented RPE, visualization of the BM was comparable across wavelengths (Figs. 2E and 2F).

Before addressing the wavelength dependence in our results, a tentative anatomical model was proposed to explain the hypo- and hyper-reflective spaces (Fig. 3A). The thickness of BM mostly comprises elastic and collagenous layers [2], which are probably highly scattering [9,15] (Fig. 3A). Therefore, the hyper-reflective band, outer to the RPE and inner to the CC, is designated as BM (Fig. 3A). The BM band was thicker in the human (Figs. 1E and 1F) than in the albino mouse (Figs. 2E and 2F), consistent with previous morphometry based on electron microscopy [16]. Given this attribution, what is the origin of the hypo-reflective "gap" between the RPE and BM bands? As the RPE basal laminar thickness [2] is only about 0.15 micrometers, too thin to resolve even by visible light OCT, we propose that the gap includes the basal portion of the RPE that does not contain melanosomes, as melanin concentrates in the apical RPE [17] (Fig. 3A), particularly in young eyes [8,18,19]. The albino mouse images strongly suggest low reflectivity of RPE constituents, including nuclei, mitochondria, and lipofuscin, in the absence of melanin (Fig. 2E).

Based on this proposed anatomical model, we hypothesized that BM is obscured in longer wavelength OCT images by multiply scattered light from melanin-containing melanosomes, because the tortuous path length of multiply scattered light overlaps with the direct path length of underlying structures, i.e., BM. It is well accepted that melanin absorption increases sharply with decreasing wavelength, from the NIR to

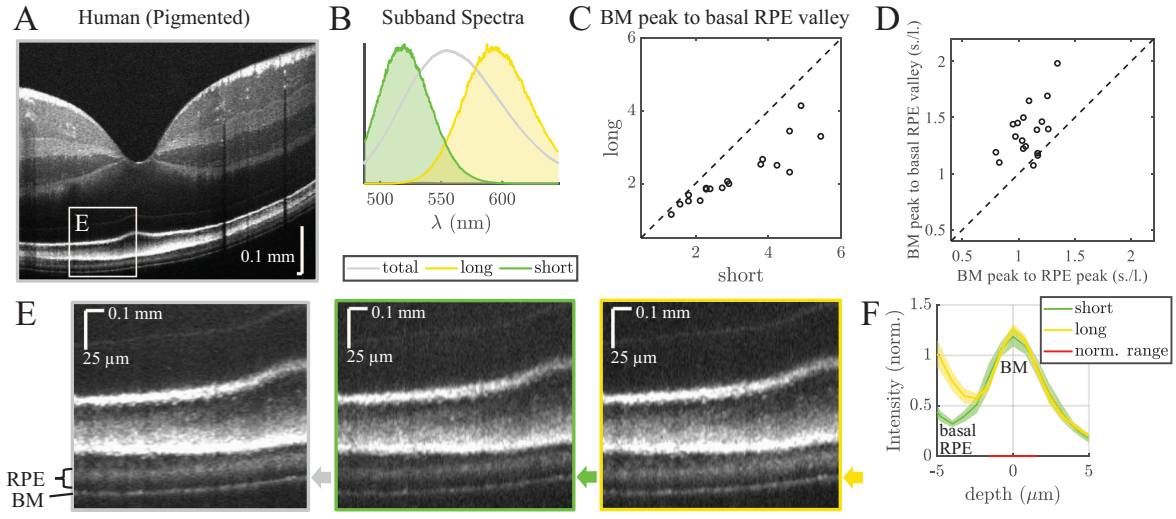

Fig. 1. Shorter wavelengths improve BM contrast, defined as the intensity ratio of the BM peak to the basal RPE valley, in the pigmented human eye. A, cross-sectional visible light OCT retinal images of a pigmented human. B, to investigate the wavelength dependence of contrast, the total spectrum (depicted in gray) was divided into two subbands centered at long (depicted in orange) and short (depicted in green) wavelengths. The two subbands (scaled here to facilitate visual comparison) were shaped to yield equivalent axial resolutions. C, BM contrast in all subjects improved at shorter OCT wavelengths in the fovea and parafovea. D, the wavelength dependence of the BM peak to basal RPE valley ratio was generally greater than that of the BM peak to RPE peak ratio, suggesting that BM contrast is not simply explained by RPE reflectivity. Outer retinal zooms (E) and intensity profiles with shaded standard errors (F) in a single subject, included in C, confirm clearer distinction between the basal hypo-reflective RPE band and BM (arrow) for green light than for orange light. The observation that shorter wavelength visible light OCT better delineates BM in pigmented eyes [Figs. 1C–1F and Figs. 2B and 2C] may relate to the general ability of visible light OCT [12] to distinguish BM more clearly than NIR OCT [13].

the ultraviolet [20]. It has recently been suggested that melanosome anisotropy decreases with wavelength [6]. Hypothesizing that both effects may diminish detection of multiply scattered light, we next performed a Monte Carlo simulation [21] (Figs. 3B–3D). We identified three approaches to determine RPE optical properties (1) simulate optical properties of single melanosomes [6] and scale based on ultrastructural density [8], (2) estimate absorption based on thermal damage thresholds [22–24], and (3) estimate all optical properties with integrating spheres [25]. Unfortunately, the results of these approaches vary widely, particularly with regard to absorption. Therefore, we performed two complementary simulations; simulation 1 featured absorption differences (Fig. 3C), while simulation 2, with longer absorption lengths, featured anisotropy differences (Fig. 3D). The optical properties in both simulations were supported in the literature. A simple Fresnel reflection represented BM. A circular, collimated source with a 6 μm diameter and an identically sized detector with a polar acceptance angle of 2.5 deg were employed. The OCT depth was taken as the path length (time-of-flight times the speed of light) divided by 2, while OCT intensity was taken as the photon number. Gaussian binning of photons in time-of-flight was performed to simulate an intensity FWHM axial (depth) resolution of 1.4 μm for each subband. Based on recent scanning electron microscopy work [8], the RPE melanosome band thickness was set to 8 μm, which happens to be similar to our scattering length ($1/\mu_s \sim 9$ μm at both 520 and 590 nm), assigned based on experimental RPE measurements [6,19,25]. The simulation 1 absorption length was similar ($1/\mu_a \sim 4.7$ μm, albedo ~ 0.35 at 520 nm, $1/\mu_a \sim 7.2$ μm, albedo ~ 0.45 at 590 nm), while the simulation 2 absorption length was larger ($1/\mu_a \sim 28$ μm, albedo ~ 0.76 at 520 nm, $1/\mu_a \sim 43.2$ μm, albedo ~ 0.83 at 590 nm). In simulation 2, as suggested Ref. [6], the scattering anisotropy was reduced at longer wavelengths. As the RPE was hypo-reflective in the albino mouse (Fig. 2E), the basal RPE scattering was set to 0. Though unrealistic, this simplified our interpretation of the results, since a single scattering model predicts no signal in this region.

For both simulations, in the 4 μm gap between the melanosome band and BM [8], multiple scattering caused spurious signal (Figs. 3E and 3F), or haze. In addition to direct backreflection from BM, quasi-backreflection from BM (BM reflection with RPE scattering), contributed 7% of the BM signal for simulation 1 and 2–3% for simulation 2. These longer paths were indistinguishable from the direct path to and from BM, given the axial resolution. Both simulations confirmed that green (520 nm) light improved the contrast of the BM relative to the hypo-reflective gap in the basal RPE (Figs. 3E and 3F) by preferentially attenuating the haze. Simulation 1 (Fig. 3E) revealed that, when assessing OCT images at the depth of the BM, increased absorption of RPE melanin is beneficial if the partial path length of unwanted multiply scattered light through melanosome-rich tissue is longer than the partial path length of useful BM-backreflected light through melanosome-rich tissue. Simulation 2 (Fig. 3F) revealed that increased scattering anisotropy (g) results in more forward scattered light and fewer detected multiply scattered paths in the RPE, which also improves BM contrast. For simulation 1, eliminating absorption degraded the contrast and eliminated the improvement at short wavelengths (dotted lines in Fig. 3E), but this was not the case for simulation 2 (dotted lines in Fig. 3F), where improvement derived from light scattering anisotropy. As the basal RPE gap was varied in a physiologically plausible range from 3 to 6 μm, maintaining an 8 μm melanosome band, the ratio of short-to-long wavelength BM contrast increased from 1.03 to 1.76 (simulation 1), and 1.11 to 1.42 (simulation 2), consistent with the observed contrast range (Fig. 1D ordinate). Thus, melanin absorption and melanosome scattering anisotropy could explain the more conspicuous hypo-reflective space between the RPE and BM bands in OCT images at short visible wavelengths.

This Letter was subject to many limitations. Given the range of literature values for RPE absorption and scattering [22–26], our simulation results should be cautiously interpreted as evidence of plausibility. Our simulation used a Henyey–Greenstein

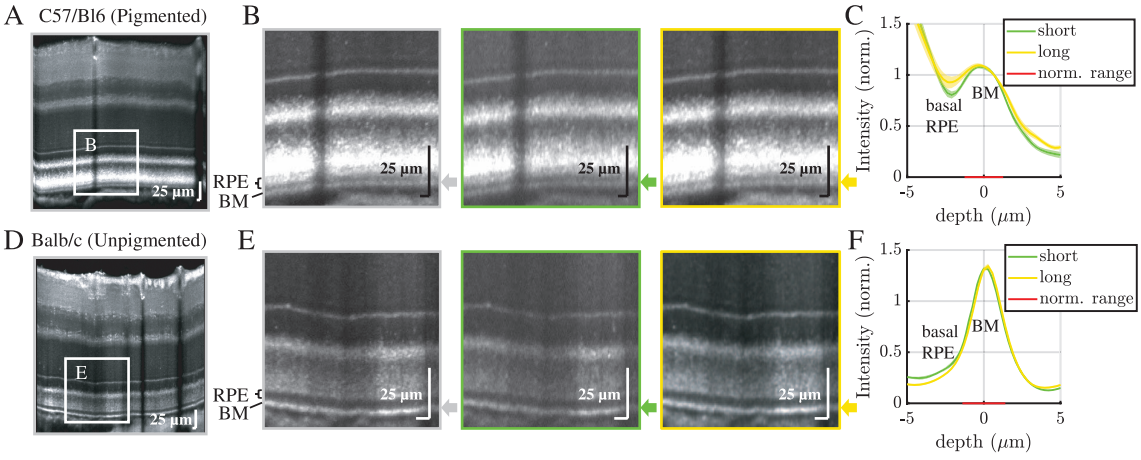

Fig. 2. Shorter wavelengths improve BM contrast, defined as the intensity ratio of the BM peak to the basal RPE valley, in pigmented mice. A, cross-sectional visible light OCT retinal image of pigmented mouse. The outer retinal zooms of the pigmented mouse (B) and intensity profiles with shaded standard errors (C) show that contrast between the basal hypo-reflective RPE and BM (arrows) is clearer for green than for orange light (see spectra in Fig. 1B). D, cross-sectional visible light OCT retinal image of unpigmented (albino) mouse. Similar zooms (E) and intensity profile (F) comparisons of the unpigmented mouse show that the RPE is hypo-reflective and, consequently, the contrast of the BM is high, with clear visualization in both subbands. These results suggest that the improved BM contrast in shorter wavelength OCT (Fig. 1) is associated with the presence of melanin.

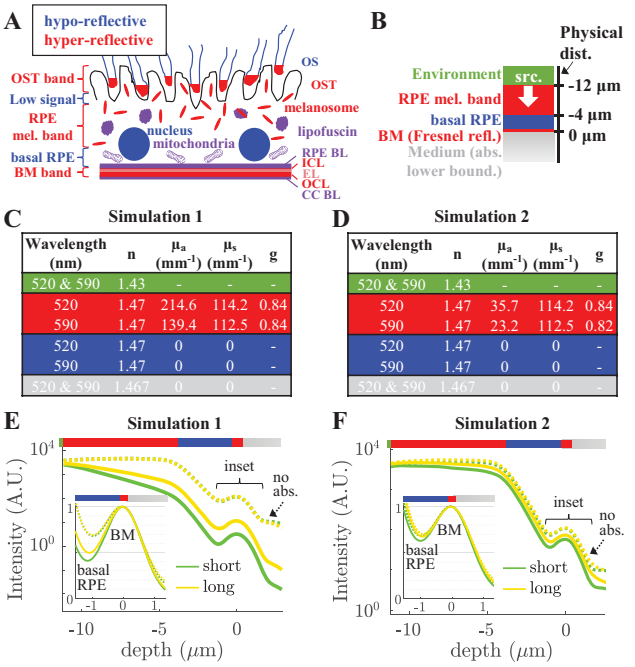

Wavelength (nm)	n	μ_a (mm^{-1})	μ_s (mm^{-1})	g
520 & 590	1.43	-	-	-
520	1.47	214.6	114.2	0.84
590	1.47	139.4	112.5	0.84
520	1.47	0	0	-
590	1.47	0	0	-
520 & 590	1.467	0	0	-

Wavelength (nm)	n	μ_a (mm^{-1})	μ_s (mm^{-1})	g
520 & 590	1.43	-	-	-
520	1.47	35.7	114.2	0.84
590	1.47	23.2	112.5	0.82
520	1.47	0	0	-
590	1.47	0	0	-
520 & 590	1.467	0	0	-

Fig. 3. A, model for RPE and BM reflectivity in visible light OCT, suggested by human (Fig. 1) and mouse (Fig. 2) data. In our model, hypothesized hyper-reflective bands are shown in red, and hypo-reflective bands are shown in blue. The majority of the BM band comprises the ultrastructural ICL, elastic layer (EL), and outer collagenous layer (OCL), while the RPE and CC basal lamina (BL) are comparatively thin. Assuming BM is hyper-reflective, the hypo-reflective space above BM must include the basal RPE cell body which contains few melanosomes. The hyper-reflective RPE band comprises melanosomes, localized in the apical RPE [27,28]. B, Monte Carlo model to simulate the depth-resolved OCT light intensity, where BM backscattering was replaced by a Fresnel reflection at the interface between the RPE and a medium with an absorbing lower boundary (gray). Two simulations were performed to encompass the range of optical properties in the literature and feature complementary effects related to absorption (simulation 1, C) and scattering anisotropy (simulation 2, D). Assumed optical properties correspond to the pigmented RPE at 520 and 590 nm, the subband central wavelengths (Fig. 1B). E and F, simulated intensity (log scale) versus depth at short and long visible wavelengths, with (solid) and without (dotted) absorption. Insets: normalized simulated intensity (linear scale) versus depth confirms the improved contrast between BM and the low signal valley of the basal RPE at shorter wavelengths, as observed in pigmented subjects (Figs. 1C–1F and Figs. 2B and 2C).

phase function, which may not accurately represent melanosome backscattering. Indeed, both simulations showed a larger RPE-to-BM intensity ratio than was observed *in vivo*. Last, changes in RPE attenuation across visible wavelengths could distort the sample spectrum, resulting in a poorer sub-RPE image resolution in the green subband. However, such an effect would have worsened BM contrast at shorter wavelengths, in contrast to our observed results.

In conclusion, visible light OCT in humans and mice suggests that melanin absorption and melanosome scattering anisotropy aid visible light OCT imaging of BM at short wavelengths. The former mechanism is reminiscent of a proposal to use absorption to aid imaging through a highly scattering wall [29], where the imaging wavelength determines absorption of the wall. Interestingly, both proposed mechanisms for contrast improvement are independent of the axial resolution, an oft-cited advantage of visible light OCT.

Funding. National Institutes of Health (EB023591, EB029747, EY012576, EY015387, EY026556, EY028287, EY031469, NS094681).

Disclosures. Vivek J. Srinivasan receives royalties from Optovue, Inc.

REFERENCES

1. C. A. Curcio, Invest. Ophthalmol. Vis. Sci. **59**, AMD160 (2018).
2. C. A. Curcio and M. Johnson, in *Retina*, S. J. Ryan, S. R. Sadda, D. R. Hinton, A. P. Schachat, C. P. Wilkinson, and P. Wiedemann, eds., 5th ed. (W.B. Saunders, 2013) Vol. **1**, pp. 465–481.
3. S. Dithmar, C. A. Curcio, N. A. Le, S. Brown, and H. E. Grossniklaus, Invest. Ophthalmol. Vis. Sci. **41**, 2035 (2000).
4. B. Lee, S. Chen, E. M. Moult, Y. Yu, A. Y. Alibhai, N. Mehta, C. R. Baumal, N. K. Waheed, and J. G. Fujimoto, Transl. Vis. Sci. Technol. **9**, 12 (2020).
5. M. Karampelas, D. A. Sim, P. A. Keane, V. P. Papastefanou, S. R. Sadda, A. Tufail, and J. Dowler, Br. J. Ophthalmol. **97**, 1256 (2013).
6. W. Song, L. Zhang, S. Ness, and J. Yi, Biomed. Opt. Express **8**, 3966 (2017).
7. B. Baumann, J. Schirmer, S. Rauscher, S. Fialova, M. Glosmann, M. Augustin, M. Pircher, M. Groger, and C. K. Hitzenberger, Invest. Ophthalmol. Vis. Sci. **56**, 7462 (2015).
8. A. Pollreisz, J. D. Messinger, K. R. Sloan, T. J. Mittermueller, A. S. Weinhandl, E. K. Benson, G. J. Kidd, U. Schmidt-Erfurth, and C. A. Curcio, Exp. Eye Res. **166**, 131 (2018).
9. S. L. Jacques, Phys. Med. Biol. **58**, R37 (2013).
10. X. Shu, L. Beckmann, and H. Zhang, J. Biomed. Opt. **22**, 121707 (2017).
11. A. Kho and V. J. Srinivasan, Opt. Lett. **44**, 775 (2019).
12. T. Zhang, A. M. Kho, and V. J. Srinivasan, Biomed. Opt. Express **10**, 2918 (2019).
13. H. Tanna, A. M. Dubis, N. Ayub, D. M. Tait, J. Rha, K. E. Stepien, and J. Carroll, Br. J. Ophthalmol. **94**, 372 (2010).
14. P. Zhang, M. Goswami, R. J. Zawadzki, and E. N. Pugh, Jr., Invest. Ophthalmol. Vis. Sci. **57**, 3650 (2016).
15. I. S. Saidi, S. L. Jacques, and F. K. Tittel, Appl. Opt. **34**, 7410 (1995).
16. S. Volland, J. Esteve-Rudd, J. Hoo, C. Yee, and D. S. Williams, PLoS One **10**, e0125631 (2015).
17. M. E. Boulton, Exp. Eye Res. **126**, 61 (2014).
18. J. J. Weiter, F. C. Delori, G. L. Wing, and K. A. Fitch, Invest. Ophthalmol. Vis. Sci. **27**, 145 (1986).
19. A. Pollreisz, M. Neschi, K. R. Sloan, M. Pircher, T. Mittermueller, D. M. Dacey, U. Schmidt-Erfurth, and C. A. Curcio, Invest. Ophthalmol. Vis. Sci. **61**, 13 (2020).
20. S. L. Jacques and D. J. McAuliffe, Photochem. Photobiol. **53**, 769 (1991).
21. L. Yu, F. Nina-Paravecino, D. Kaeli, and Q. Fang, J. Biomed. Opt. **23**, 1 (2018).
22. S. L. Jacques, R. D. Glickman, and J. A. Schwartz, Proc. SPIE **2681**, 468 (1996).
23. R. Birngruber, F. Hillenkamp, and V. P. Gabel, Health Phys. **48**, 781 (1985).
24. M. S. Schmidt, P. K. Kennedy, R. L. Vincelette, M. L. Denton, G. D. Noojin, K. J. Schuster, R. J. Thomas, and B. A. Rockwell, J. Biomed. Opt. **19**, 35003 (2014).
25. M. Hammer, A. Roggan, D. Schweitzer, and G. Muller, Phys. Med. Biol. **40**, 963 (1995).
26. C. N. Keilhauer and F. C. Delori, Invest. Ophthalmol. Vis. Sci. **47**, 3556 (2006).
27. R. S. Jonnal, O. P. Kocaoglu, R. J. Zawadzki, S. H. Lee, J. S. Werner, and D. T. Miller, Invest. Ophthalmol. Vis. Sci. **55**, 7904 (2014).
28. Z. Liu, O. P. Kocaoglu, and D. T. Miller, Invest. Ophthalmol. Vis. Sci. **57**, OCT533 (2016).
29. K. M. Yoo, F. Liu, and R. R. Alfano, Opt. Lett. **16**, 1068 (1991).